Wettability characterization method based on optical coherence tomography imaging

Tapio Fabritius,[1,*] **Risto Myllylä,**[1] **Shuichi Makita,**[2] **and Yoshiaki Yasuno**[2]

[1]*Optoelectronics and Measurement Techniques Laboratory, University of Oulu, Oulu, Finland*
[2]*Computational Optics Group, University of Tsukuba, Tsukuba, Japan*

**tapio.fabritius@ee.oulu.fi*

Abstract: A novel method for surface wetting characterization based on contact angle measurements is presented. Three dimensional structural imaging of a droplet on a substrate is performed using optical coherence tomography (OCT) which provides micrometer resolution images without contact with the sample. An automatic OCT intensity variation based, layer segmentation method was implemented to identify air-droplet, droplet-substrate and air-substrate interfaces. A glycerol droplet on a rough tilted glass substrate was used as a test sample to demonstrate the applicability of the proposed method for wetting characterization. Results show that the contact angle of any observation angle can be obtained. In addition, the droplet's average refractive index can be determined. The proposed method is an interesting and complementary tool for present wetting characterization methods.

OCIS codes: (070.5010) Pattern recognition; (100.0100) Image processing; (110.0110) Imaging systems; (110.4500) Optical coherence tomography; (120.0120) Instrumentation, measurement, and metrology.

References and links

1. G. Kumar and K. N. Prabhu, "Review of non-reactive and reactive wetting of liquids on surfaces," Adv. Colloid Interface Sci. **133,** 61–89 (2007).
2. N. K. Winter, D. M. Anderson and R. J. Braun, "A model for wetting and evaporation of a post-blink precorneal tear film," Math. Med. Biol. **27,** 211–225 (2010).
3. L. V. Chasovnikova, V. E. Formazy , V. I. Sergienko, and Yu. F. Maichuk, "Surface Activity and Wetting Effect of Artificial Tear Preparations," Bull. Exp. Biol. Med. **115,** 387–389 (1993).
4. K. L. Menzies, R. Rogers, and L. Jones, "In Vitro Contact Angle Analysis and Physical Properties of Blister Pack Solutions of Daily Disposable Contact Lenses," Eye Contact Lens **36,** 10–18 (2010).
5. Y. J. Lim and Y. Oshida, "Initial contact angle measurements on variously treated dental/medical titanium materials," Biomed. Mater. Eng. **11,** 325–341 (2001).
6. M. J. Yaszemski, D. J. Trantolo, K. Lewandrowski, V. Hasirci, D. E. Altobelli, and D. L. Wise, *Biomaterials in orthopedics*, (Marcel Dekker, USA, 2004).
7. J. Bei, W. Wang, Z. Wang, and S. Wang, "Surface Properties and Drug Release Behavior of Polycaprolactone Polyether Blend and Copolymer," Polym. Adv. Technol. **7,** 104–107 (1996).
8. M. Ardhaoui, M. Nassiri, M. Rubaei, D. Dowling, "Influence of water contact angle on cell adhesion on polystyrene surfaces," presented at the NanoTech conference, Boston, USA, 1–5 June (2008).
9. M. Sun, G. S. Watson, Y. Zheng, J. A. Watson, and A. Liang, "Wetting properties on nanostructured surfaces of cicada wings," J. Exp. Biol. **212,** 3148–3155 (2009).
10. A. M. Zysk, F. T. Nguyen, A. L. Oldenburg, D. L. Marks, and S. A. Boppart, "Optical coherence tomography: a review of clinical development from bench to bedside," J. Biomed. Opt. **12,** 051403 (2007).

#134530 - $15.00 USD Received 2 Sep 2010; revised 6 Oct 2010; accepted 8 Oct 2010; published 13 Oct 2010

11. F. Jaillon, S. Makita, M. Yabusaki, and Y. Yasuno, "Parabolic BM-scan technique for full range Doppler spectral domain optical coherence tomography," Opt. Express **18,** 1358–1372 (2010)
12. T. Fabritius, S. Makita, M. Miura, R. Myllylä, and Y. Yasuno, "Automated segmentation of the macula by optical coherence tomography," Opt. Express **17,** 15659–15669 (2009).
13. N. Otsu, "A threshold selection method from gray-level histograms," IEEE Trans. Syst. Man Cybern. **9,** 62–66 (1979).
14. G. J. Tearney, M. E. Brezinski, J. F. Southern, B. E. Bouma, M. R. Hee, and J. G. Fujimoto "Determination of the refractive index of highly scattering human tissue by optical coherence tomography," Opt. Lett. **20,** 2258–2260 (1995).
15. L. Gao and T. J. McGarthy, "Wetting 101 $^{\circ\dagger}$," Langmuir **25,** 14105–14115 (2009).
16. A. Marmur and E. Bittoun, "When Wenzel and Cassie Are Right: Reconciling Local and Global Considerations," Langmuir **25,** 1277–1281 (2009).
17. L. Gao and T. J. McGarthy, "An Attempt to Correct the Faulty Intuition Prepetuated by the Wenzel and Cassie "Laws"," Langmuir **25,** 7249–7255 (2009).
18. T. Fabritius and R. Myllylä, "Liquid sorption investigation of porous media by optical coherence tomography," J. Phys. D Appl. Phys. **39,** 4668–4672 (2006).
19. T. Fabritius and R. Myllylä, "Investigation of swelling behaviour in strongly scattering porous media using optical coherence tomography," J. Phys. D Appl. Phys. **39,** 2609–2612 (2006).

1. Introduction

Wetting of a solid by a liquid is a complicated process having an important role in our everyday life. A large number of biological and industrial processes involve wetting phenomena. Wettability is describing a tendency of a liquid to spread on a solid substrate and is measured in terms of the angle between the tangent drawn at the connection point of the three phases (solid, liquid and vapour) and the substrate surface [1]. Some applications need a good wetting between liquid and substrate surface whereas others require poor wetting or even repellency. In order to understand the fundamentals of the behavior and properties of materials and biological systems, an effective approach to investigate wetting is contact angle (CA) measurement [1].

Based on CA measurements, we can examine the evolution of a precorneal tear film [2] and develop better artificial tears [3] and more comfortable contact lenses [4], improve the design of biocompatible implants for dentistry and medicine [5, 6] or improve the drug release properties of developed drugs [7]. We can understand which kinds of structures are optimum for cell adhesion [8] or why the fore wings of cicada do not get wet in rain [9].The list of examples can be continued almost infinitely, clearly indicating the essential role of wetting phenomena in biology and medicine not forgetting its importance in other fields as well [1].

Perhaps the most commonly used CA measurement technique is the so-called goniometric based method in which the CA is obtained using an optical subsystem to capture the profile of a liquid on a solid substrate. Modern systems employ high resolution cameras and software to capture and analyze the CA. Present CA measurement methods, have however some applicability limitations for wetting evaluation. They don't provide the possibility to directly investigate what happens underneath the droplet and they are not that reliable if the substrate is very rough, curved or chemically unhomogeneous. That is why present methods are not always suitable for the wetting characterization of biological systems, especially if *in vivo* characterization is needed.

Optical coherence tomography (OCT) is an optical imaging method which has been widely used in numerous applications in the biomedical field including ophthalmology, dermatology, cardiology, gastroenterology, etc [10]. OCT is an effective research tool enabling high resolution, three-dimensional *in vivo* imaging of biological tissues in a non-invasive and safe manner. Previous OCT research has mostly focused on structural characterization, but thanks to the technical development of OCT, investigations into the dynamic phenomena have recently increased. Taking into consideration the advantageous properties of OCT, we believe that it would be very suitable for wetting characterization.

#134530 - $15.00 USD Received 2 Sep 2010; revised 6 Oct 2010; accepted 8 Oct 2010; published 13 Oct 2010

To overcome the limitations of available CA measurement methods, an alternative methods for that purpose is required. The main ambition of this work is to demonstrate an alternative CA measurement concept and discuss the capabilities of OCT for CA determination which will, in turn, highlight a new field of application.

2. Method

2.1. Measurement System

Spectral domain OCT (SD-OCT) based on the unbalanced Michelson interferometer is used. By utilizing a broadband SLD light source with 1.020 μm central wavelength and 100 nm spectral width, high resolution imaging (axial resolution $\sim$6 μm) of a droplet on the substrate can be achieved. A high-speed InGaAs line scan camera with 1024 pixels enables a detection speed of 47,000 axial scans/s with 98.5 dB sensitivity. A more detailed description of the measurement device can be found elsewhere [11]. The scanner of that system was replaced by a setup which scans perpendicularly to the sample plane. A glycerol droplet on a rough glass plate is used as a test sample.

2.2. Data Processing

After standard OCT data processing an interface segmentation is performed to identify the shape of the droplet. The developed automatic segmentation method is based on the intensity variations of the logarithmic OCT intensity signal. Algorithm identifies the position of air-substrate (A-S), air-droplet (A-D) and droplet-substrate (D-S) interfaces from a measured three dimensional (3D) data set. The presented method is inspired by the previously published OCT data segmentation method [12]. The schematic of developed segmentation method is shown in Fig. 1.

The OCT signal intensity of each A-scan in measured data volume is described with $\{I(x,y,z), x \in [1,M], y \in [1,N]\}$, where z refers to the depth position of a pixel from the beginning of the depth scan. N is the position of A-scan in each B-scan and M is the position of the B-scans. Thus $M \times N$ is the total number of A-scans in the processed data volume.

The first step in the automatic process is the determination of the depth position of maximum intensity pixels of each A-scan; $\{max(I_{x,y}(z))\}$. Due to the fact that the intensity of the obtained OCT signal is proportional to the refractive index difference between the optical interfaces, the maximum intensity pixels are positioned at the segmented interface. In our case, maximum intensity pixels were located at A-S and D-S interface. See image after step (i) in Fig. 1. The positions of each of the maximum intensity pixels are stored in the a 2D matrix $Z_{ASDS}(x,y)$.

Due to the speckle noise and signal distortion caused by saturation of the detector used, some pixels are erroneously positioned outside the determined interfaces. To make position identification of erroneous pixels easier, the obtained 2D position matrix $Z_{ASDS}(x,y)$ is processed by moving median filtering (size 10(x)$\times$10(y) pixels) and bot-hat filtering which computes the morphological opening of the image and then subtracts the result from the original image. The size of the used structuring element was 50(x)$\times$50(y) pixels. To obtain a mask $Mask_{ASDS}(x,y)$ that can be used for identifying the position of erroneous pixels in a $Z_{ASDS}(x,y)$ matrix, the bot-hat filtered position matrix is thresholded by automatic binarization algorithm, based on Otsu's method (step (ii)) [13]. All the pixels in a position matrix which are expected to be erroneous are set to be without any numerical value so-called NaN value. All elements of the matrix with NaN (if $Mask_{ASDS}(x,y) = 0$ then $Z_{ASDS}(x,y) = NaN$) value are replaced by numerical value based on the contextual information of neighboring pixels (step (iii)) and smoothened by the moving window median filter (size 3(x)$\times$100(y) pixels).

Now the determined position matrix $Z_{ASDS}(x,y)$ contains information regarding the A-S and the D-S interfaces. To distinguish them from each other, the contact area of droplet with sub-

#134530 - $15.00 USD Received 2 Sep 2010; revised 6 Oct 2010; accepted 8 Oct 2010; published 13 Oct 2010

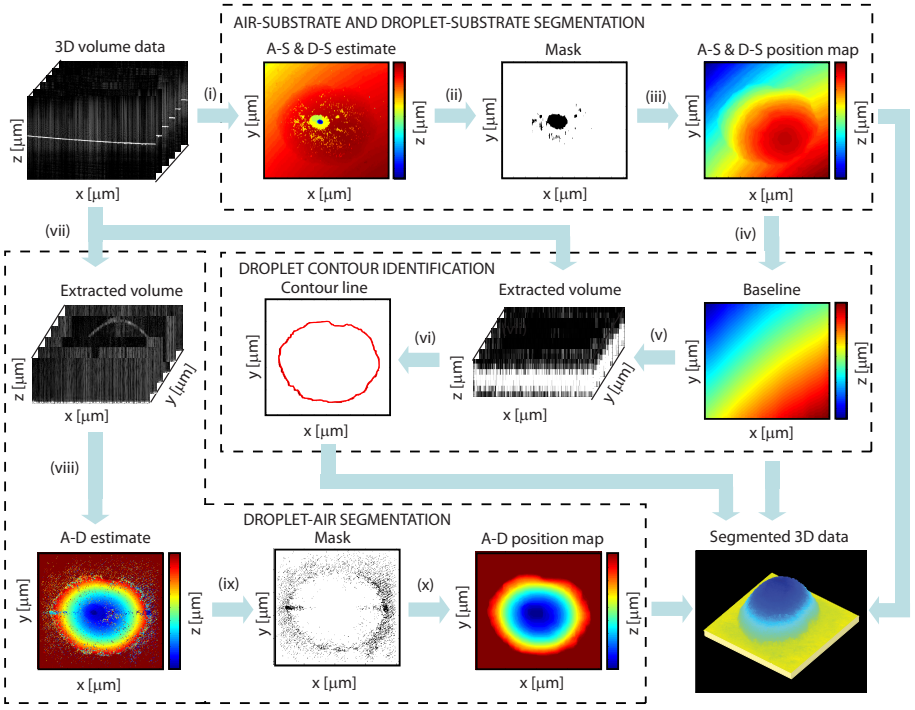

Fig. 1. Schematic of 3D segmentation of A-D, A-S and D-S interfaces. Steps i-ii are for A-S and D-S segmentation, iv-vi are for baseline identifications and vii-x are for A-D segmentation. Light blue arrows depict information flow during segmentation.

strate is determined. It was assumed that the measurement area covers the whole droplet. Thus, we can expect that pixels on the edge of the above-mentioned position matrix belongs to the A-S interface. Pixels from the edge of position matrix $Z_{ASDS}(x,y)$ are extracted to a separate matrix $Z_{as}(x,y)$ and all pixels inside the edges are set to be NaN. Using the linear interpolation method, all the NaNs are replaced by numerical value. Thus matrix $Z1_{as}(x,y)$ can be regarded as an estimation for physical depth position for the first interface of substrate (step (iv)).

Six pixels around $Z1_{as}(x,y)$ are extracted from the original data volume $\{I(x,y,z),\ z \in [Z1_{as}(x,y)-3,\ Z1_{as}(x,y)+3]\}$ (step (v)) and depth oriented integration of the extracted volume, and the so-called projection image $Proj(x,y)$ is calculated. The obtained projection image is blurred by the moving median filter (size 20(x)×3(y) pixels) and binarized using Otsu's method. Morphological closing (structuring element 15(x)×15(y)) and opening (structuring element 50(x)×50(x)) operations of the binarized image are sequentially performed to remove all shapes that do not belong to the contact line of the droplet. The contact line pixels are determined using outline tracking algorithm, in which nonzero pixels belong to an object (in our case the contact area of the droplet) and zero pixels constitute the background. The positions of pixels on the contact line are denoted as (x_i,y_i) where i indicates the index of the pixels (step vi).

As the shape of the contact area of the droplet is known, the pixels belonging to A-S interface can be extracted from the measurement data. Knowledge of the droplet shape also allows us to

#134530 - $15.00 USD Received 2 Sep 2010; revised 6 Oct 2010; accepted 8 Oct 2010; published 13 Oct 2010

determine the center of the droplet (x_{center}, y_{center}). The principle of that operation is the same as the object's center of gravity determination, which is determined as the center of gravity of the region determined by the contact line. The radius r_i of the droplet is determined by calculating the Euclidean distances of the contact line pixels from the center of the droplet $r_i = \sqrt{(x_{center} - x_i)^2 + (y_{center} - y_i)^2}$.

The last step of droplet shape determination is the A-D interface identification. Now the 45 pixels above the baseline $Z1_{as}(x,y)$ are extracted and the maximum intensity of each depth scan is determined. The depth position of maximum intensity pixels is stored by matrix $Z_{ad}(x,y)$ and smoothened by a moving median filter (size 1(x)×100(y) pixels) to get matrix $Z1_{ds}(x,y)$ (steps(vii and viii)). The matrix $Z_{ad}(x,y)$ is subtracted from matrix $Z1_{ad}(x,y)$ and the obtained matrix is binarized according to Otsu's method to obtain a mask (step (ix)) which is used to determine the position of erroneous pixels. Using this the erroneous pixels in matrix $Z_{ad}(x,y)$ are set to be NaN. All the NaN values are replaced to estimated values based on the values of the nearest neighboring pixels and the obtained matrix is smoothened by moving average median filters (20(x)×1(y) and 1(x)×300(y)) to obtain the position matrix for A-D interface $Z_{AD}(x,y)$ (step(x)).

The contact angle is determined by using $Z_{AD}(x,y)$. Pixels between the center of the droplet and the contact line, which is the height profile of the droplet, are extracted and fitted by a second order polynomial. At a point where the A-D surface meets the substrate surface, the tangent of that curve is calculated and the angle between the substrate and obtained tangent is determined. This angle corresponds to the contact angle of the droplet. The same procedure is repeated on the all pixels in the contact line matrix in order to have contact angle distribution as a function of observation angle.

Segmentation algorithms are implemented in Matlab and the whole data processing is performed by a normal personal computer. The required calculation time was around 2.5 min for the whole data processing.

3. Results

To validate the method proposed, a glycerol drop on a tilted (4.1°) ground glass plate was examined. All CA measurements were performed at normal room temperature and humidity and the used substrates were not prepared before measurement. The size of the measured area was 1.7×1.7 mm^2 and measurement depth was 1.4 mm, yielding data cubes containing 2048×400×256 pixels. The required measurement time for the data set was 11.2 s.

The obtained data set was processed by the method described above. A summary of the OCT measurement results is depicted in Fig. 2, and a summary on analysis is presented in Fig. 3. Three-dimensional volume rendering with a projection image is shown on the left side of Fig. 2. Based on the projection image, the contact area of a droplet was automatically determined. The distance from the center of the droplet to the boundary of the contact area, namely the radius of the droplet, was obtained. In addition, cross-sectional images were extracted from the data volume to do more detailed investigation of the contact angle.

The mean radius was measured to be 0.68±0.05 mm (mean±standard deviation) while the CA was measured to be 10.7°±0.8° (mean±standard deviation). The variation of radius and contact angle is mainly caused by the tilting of the glass plate and the roughness of the substrate. This also explains why the shape of a droplet on rough glass is not a perfect circle [Fig. 3(a)] but more like an ellipse.

The results shown in Figs. 3(c) and 3(d) show evidence of negative correlation between droplet radius and contact angle. The calculated correlation coefficient was -0.827. Due to the limited imaging resolution of the OCT system used and possible segmentation errors, the accuracy of the determined contact angle is probably inferior to conventional methods. However, the

#134530 - $15.00 USD Received 2 Sep 2010; revised 6 Oct 2010; accepted 8 Oct 2010; published 13 Oct 2010

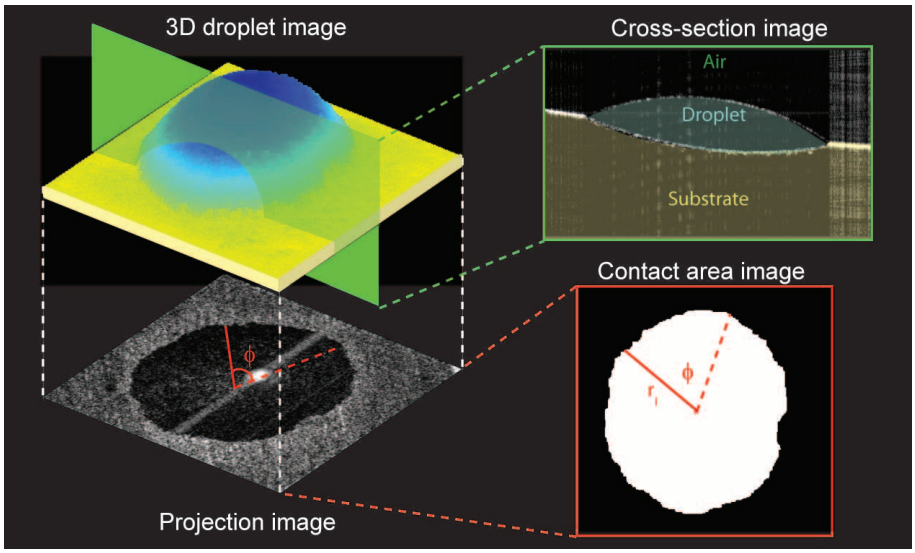

Fig. 2. Three dimensional investigation of a droplet on a solid substrate. Both cross-sectional image and projection image can be calculated for evaluating the liquid wetting and sorption properties.

presented method is applicable for samples which cannot be measured reliably by conventional methods, e.g. samples with high isotropic roughness or highly curved substrate.

In addition to contact angle measurements, the average refractive index of the droplet was determined. Due to the different optical path lengths of photons traveling in air and in glycerol, the glass surface seems to be bended beneath the droplet [Fig. 3(b)]. The refractive index of droplet $n = (L_1 + L_2)/L_1$ [14] was determined from the A-line, in which the droplet surface is normal to the probe beam and it was measured to be 1.46. That correlates well with the refractive index of glycerol in the literature ($n_g = 1.466$).

In order to have a reference to our CA measurements, we made a goniometric type CA measurements (Grüss, DSA100) with the same glass substrate and liquid. In Fig. 4(a), a selected case of goniometric type CA measurement is shown. The procedure was repeated ten times and the mean CA was measured to be $13.7^\circ \pm 2.7^\circ$ (mean $\pm$ standard deviation), varying between 10.5° and 19.2°. Results also show the typical tendency of goniometric CA method to have a large variation of measured CA values. Obtained goniometrically determined CA value is in the same order of magnitude as OCT based CA analysis. It should be noted that goniometric and OCT based measurements are performed for different droplets.

Scanning electron microscopy (SEM) (JEOL, JCM-5000 NeoScope) imaging of used glass substrate was also performed to obtain a better understanding of surface roughness properties. The obtained results [Fig. 4(b)] show that the average surface feature size is around 20 μm. The isotropic nature of surface roughness is clearly seen in Fig. 4(c).

4. Discussion

The proposed method provides CA as a function of radial angle. In contrast, conventional CA determination methods usually provide only a single representative contact angle value. As shown in Section 3, the CA varies with in a certain range. In our case, a total variation range was 4.2° when the average CA was around 11°. These facts imply the limited applicability of the conventional method and the advantage of the proposed method. Another disadvantage of

#134530 - $15.00 USD Received 2 Sep 2010; revised 6 Oct 2010; accepted 8 Oct 2010; published 13 Oct 2010

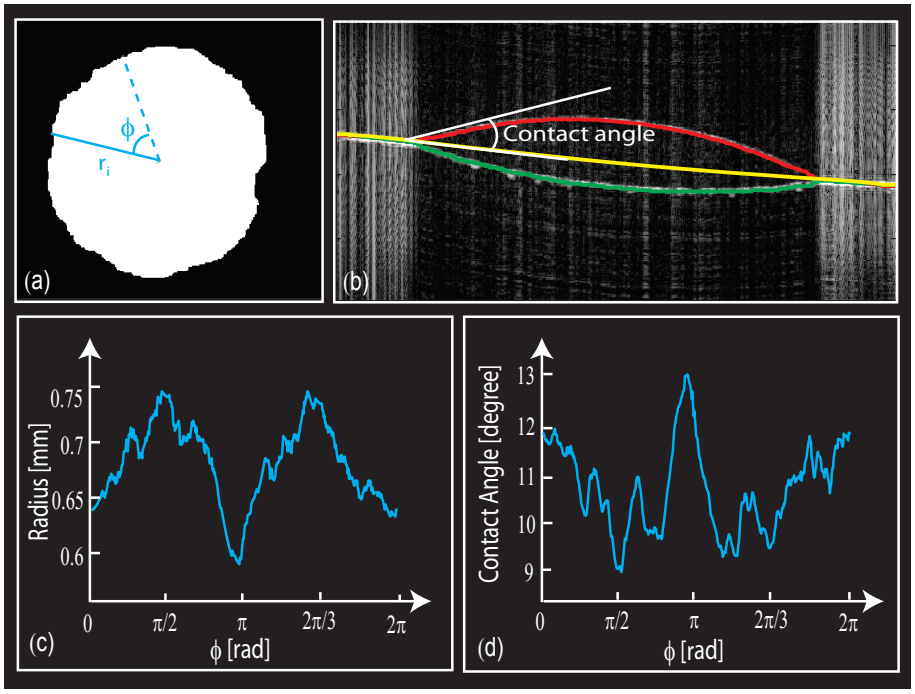

Fig. 3. (a) Contact area between the droplet and substrate, (b) cross-sectional image with identified interfaces, (c) the radius of the droplet as a function of radial angle ϕ, and (d) contact angle as a function radial angle ϕ.

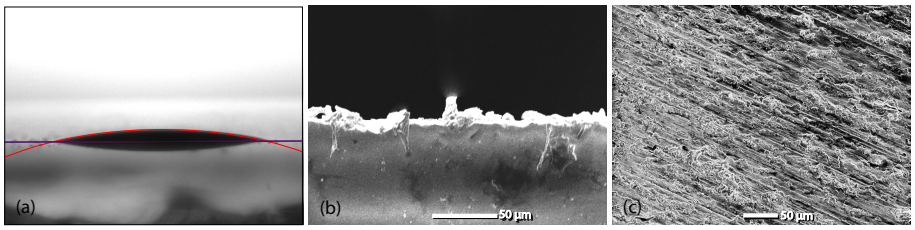

Fig. 4. (a) Contact angle measurement by conventional goniometric device, (b) cross-section image of substrate with 500 times magnification by SEM, (c) surface image of substrate with 500 times magnification by SEM.

conventional methods, particularly goniometric type methods, is the dependency of the measured CA value on the observation angle. It is worth mentioning that OCT is not affected by this problem.

Some conventional methods provide advancing and receding CA values to evaluate wetting properties [15]. However, those values present only extreme cases, which may not well reflect the practical wetting property of a sample. If we want to have more exact and realistic properties of liquid wetting in certain conditions, the measurement of advancing and receding CA values are not sufficient. Also, from this point of view, the presented OCT based method has clear advantages compared with other methods available.

As typical goniometric CA measurements are performed, the manual intervention of the operator is often needed to get reliable results, which causes unwanted variations in CA results

#134530 - $15.00 USD Received 2 Sep 2010; revised 6 Oct 2010; accepted 8 Oct 2010; published 13 Oct 2010

obtained by different operators. A typical problem is the baseline identification [blue horizontal line in Fig. 4(a)], which very often needs to be done manually because the contrast between air and substrate is not sufficient. In the case of the proposed method, the whole CA analysis is totally automated and it does not suffer from that problem at all.

At the moment, the opinions of researchers concerning the effect of different factors on wetting properties are not totally consistent [15–17]. It has been shown that from the wetting characterization point of view, the contact line is one of the most important factors having a bearing upon it. However, the substrate properties beneath the droplet also seem to have an impact on wetting phenomena. Further development of the OCT based method might enable simultaneous investigation of contact line, contact area and CA.

Wetting phenomena can become even more complicated as the liquid is able to penetrate into the substrate, or chemically interact with the substrate. Penetration may happens if pores and capillaries exist in the substrate and chemical reaction occurs if the interactive materials are non-inert with each other. In these cases, the investigation of D-S interface will be important. Previous studies have shown that OCT technology can visualize liquid penetration into a sample in depth direction [18] and can investigate the interaction between the liquid and the substrate material [19]. The simultaneous measurements of liquid penetration and CA may be an interesting future project. Since the liquid penetration into the sample is usually a very fast process, high imaging speed is required. Development of ultra-high-speed OCT technology might enable these kinds of investigations.

The proposed algorithm worked correctly for the applied data set and the obtained CA values are consistent with goniometric type CA measurement results. These facts indicate that the proposed method is feasible for wetting characterization. However, more detailed investigation of the repeatability and accuracy of that method is definitely needed.

5. Conclusion

In this paper we have demonstrated a new OCT based method to determine the wettability of homogeneous and heterogeneous substrates. Although this method is based on traditional contact angle measurements, it has overcome certain limitations of current wetting characterization methods. This method may extend the limit of investigation of wettablity.

Acknowledgement

This study is partially supported by the Japan Science and Technology Agency through the contract of the development program of advanced measurement systems.

#134530 - $15.00 USD Received 2 Sep 2010; revised 6 Oct 2010; accepted 8 Oct 2010; published 13 Oct 2010